Volume 18, Number 2, 2025. pp. 123-130

Jordan Journal of Physics

ARTICLE

Study of the Nuclear Structure for the ^{19}O Nucleus by Using USDEPN and WCPN Interactions

Hadeel H. Abed[a] and **Ali K. Hasan**[b]

[a] *Department of Physics, College of Education for Girls, University of Kufa, Iraq.*
[b] *College of Health and Medical Technology, University of Alkafeel, Iraq.*

Doi: **https://doi.org/10.47011/18.2.2**
Received on: 18/08/2023; *Accepted on: 14/04/2024*

Abstract: The NuShellX@MSU code, along with the USDEPN and WCPN interactions within the sdpn-shell model space, has been employed to study the energy levels, electromagnetic transition probabilities, and charge density distribution of the ^{19}O nucleus using the nuclear shell model. The model space for this under-researched nucleus contains the configurations ($0d_{5/2}$, 1s1/2, and 0d3/2). In terms of energy levels, a generally acceptable agreement was achieved for several states, while a comparable similarity is anticipated for others. As for electromagnetic transfers, the default values of the effective charge and the g-factors were changed to obtain an acceptable agreement with the experimental magnetic transfer data for the ground state. However, no experimental data for the charge density distribution are currently available for comparison..

Keywords: ^{19}O nucleus**,** Electromagnetic transitions, Charge density, Sdpn-shell.

PACS: 21.60.Cs.

1. Introduction

Several models have been devised to explain the structure of atomic nuclei. One such model is the nuclear shell model (SM), which has been extensively studied. First proposed by Mayer, Haxel, Jensen, and Suess almost half a century ago, this model has been highly effective in explaining the characteristics of different nuclei that have only a small number of valence nucleons. The features encompassed are energy levels, magnetic and electrical moments, electromagnetic transmission possibilities, and the cross-section of different reactions [1]. The shell model is one of the most well-known and useful nuclear models, which can help us understand nuclear structure, which contains the fundamental physical properties of nuclei. The electron shell model of atoms is comparable to this idea. Nucleons, either protons or neutrons, situated beyond closed shells (defined by magic numbers 2, 8, 20, 28, 50, 82, and 126), exert significant influence on shaping nuclear properties, much like the way valence electrons outside a closed shell define atomic traits and behaviors. Nuclei marked by magic numbers are exceptionally stable and display wholly distinctive attributes when contrasted with other nuclei [2].

All shell-model computations commence by deriving an effective interaction, founded on a microscopic theory originating from the free nucleon-nucleon (N-N) interaction. Consequently, these extensive shell-model computations enable us to gauge the extent to which a two-body effective interaction replicates attributes such as excitation spectra and binding energies in scenarios involving numerous valence nucleons. Within a constrained domain known as the model space, a subset of the complete Hilbert space, the challenges of

Corresponding Author: Ali K. Hasan **Email**: alikh.alsinayyid@alkafeel.edu.iq

acquiring such effective operators and interactions are resolved. Various avenues exist to expand effective operators and interactions. As an illustration, the Cohen-Kurath interaction is applied within the p-shell for nuclei with 4 < A < 16, while the USD interaction has its suitability in the SD-shell for nuclei with 16 < A < 40 [3]. Nuclear shell model codes like Oxbash [4], Antoine [5], NuShell [6], NuShellX [7], and others have been widely employed for shell-model calculations in the p-shell, sd-shell, and fp-shell. These codes play a crucial role globally in scrutinizing nuclear structure. Basic inputs for most shell-model configuration mixing codes (TBMEs) involve sets of single-particle matrix elements (SPEs) and two-body matrix elements. These sets are characterized as "model-space Hamiltonians" or "effective interactions" [8]. The present study employed the NuShellX@MSU code to compute energy levels, electromagnetic transitions, and charge density distribution for the ^{19}O nucleus. This was accomplished using the USDEPN and WCPN interactions within the sdpn-shell. Previous theoretical research has been conducted on the studied isotope [9].

2. Theory

NuShellX@MSU encompasses a series of wrapper scripts developed by Alex Brown [7], designed to generate input for NuShellX using model space and Hamiltonian data files. With the aim of computing precise energies, eigenvectors, and spectroscopic overlaps for low-lying states within calculations that involve the shell-model Hamiltonian matrix featuring remarkably expansive basis dimensions, Bill Rae [6] engineered a suite of computer programs recognized as NuShellX.

In the context of the shell model framework, the Hamiltonian of a system comprising A nucleons is decomposed using an auxiliary one-body potential U. This potential is composed of two parts: H_0, representing the independent motion of the nucleons, and H_1, the residual interaction. Thus [10, 11]:

$$H = \sum_{i=1}^{A} \frac{p_i^2}{2m} + \sum_{i<A=1}^{A} V_{ij}^{NN} = T+V = (T+U) + (V-U) = H_0 + H_1 \quad (1)$$

where:

$$H_0 = \sum_{i=1}^{A} \left(\frac{p_i^2}{2m} + U_i\right) \quad (2)$$

$$H_1 = \sum_{i<A=1}^{A} V_{ij}^{NN} - \sum_{i=1}^{A} U_i \quad (3)$$

Once H_0 is introduced, a reduced model space can be delineated by employing a finite subset of HO's eigenvectors [10].

Numerous theories exist to determine the permissible total angular momentum, such as when nucleons (neutrons or protons) are present in a single orbit with n > 2, where n represents the count of particles beyond the closed shell. In this case, the total angular momentum is given by[12]:

$$J_M = n\left[j - \frac{(n-1)}{2}\right] \quad (4)$$

To calculate the physical factor for systems that contain several particles, I followed the method of expressing the total wave function of the group of particles in terms of the wave function of one or two particles, depending on the nature of the physical quantity to be calculated. Using certain mathematical methods, there may be a need to separate the total wave function into the wave function for more than two particles and the wave function for the remaining particles. This is done using specific mathematical methods [13]. To illustrate the computation of a nucleus's spectrum where valence nucleons all occupy a single-particle state, we need to introduce the notion of parentage coefficients. In essence, we introduced the fractional parentage method as a means to calculate the matrix elements of the interaction. Through this technique, we were able to express the condition of having n particles in terms of states involving (n - 1) or (n - 2) particles. In the configuration j^n, the anti-symmetric state with angular momentum (JM) is represented by $\psi_{JM\alpha}$ (1,..., n). The single-particle eigenfunction for the state j is labeled as |jm⟩ or φ_{jm}, and α represents an additional quantum number required for full specification of the state. In instances where the configuration j^{n-1} is composed of entirely anti-symmetric wave functions, they are denoted as $\phi_{J_1 M_1 \beta_1}$, $(1, \ldots\ldots, n-1)$, and we can accordingly formulate these as [14]:

$$\psi_{JM\alpha}(1, \ldots, n) = \sum_{J_1\beta_1} [j^{n-1}\beta_1 J_1) jJ|\}j^n \alpha J][\phi_{J_1\beta_1}(1, \ldots\ldots, n-1) \times \varphi_j(n)]_{JM} \quad (5)$$

The real expansion coefficients, denoted as $[j^{n-1}\beta_1 J_1) jJ|\}j^n \alpha J]$, are referred to as fractional parentage coefficients (c.f.p.). These coefficients

are determined in such a way that the n-particle wave function becomes anti-symmetric when any two particles are interchanged, including both β and α [15, 16].

A second type of parentage coefficient is called a double parentage coefficient, or d.p.c., and it is described as follows: If $\varphi_{KM_2'}$ $(n$ -1, $n)$ denotes all two-particle state $(j^2)_{KM_2'}$, and $\phi_{J_2M_2\beta_2}(1, \ldots \ldots n-2)$ is the entire set of anti-symmetric states of j^{n-2}, then the anti-symmetric state of the configuration j^n with angular momentum JM can be written in the following form [17]:

$$\psi_{JM\alpha}(1,..,n) = \sum_{J_2\beta_2K}[j^{n-2}\beta_2J_2)j^2(K)J|\}j^n\alpha J][\phi_{J_2\beta_2}(1,\ldots,n-2)\times\varphi_K(n-1),n]_{JM} \quad (6)$$

Thus, when there are more than two particles outside the closed shell (n > 2) and these particles occupy the same level, the energy matrix element or the Hamiltonian matrix element is given by [14, 17, 18]:

$$\langle H\rangle = n\varepsilon_j\delta_{\alpha\alpha'} + \left\{\frac{n}{n-2}\right\}\sum_{J_1\beta_1\beta_1'}[j^{n-1}(\beta_1'J),jJ|\}j^n\alpha'J] \times [J^{n-1}(\beta_1J_1),jJ|\}j^n\alpha J] \times \langle jj|V|jj\rangle_{J_1} \quad (7)$$

In an alternative explanation, Eq. (7) articulates how the matrix elements of two-particle operators within the n-particle configuration can be understood as linear constituents within the matrix configuration of (n-1)-particle combinations. Given the time-intensive nature of this procedure, introducing the concept of d.p.c. offers a more streamlined resolution. If these coefficients are available, the subsequent formula is applicable for calculating the energy of the state $(j)_J^n$ [14, 17, 18]

$$\langle H\rangle = n\varepsilon_j\delta_{\alpha\alpha'} + \left\{\frac{n(n-1)}{2}\right\}\sum_{\beta_2J_2K}[j^{n-2}(\beta_2J_2),j^2(K)J|\}j^n\alpha'J] \times [J^{n-2}(\beta_2J_2),j^2(K)J|\}j^n\alpha'J] \times \langle jj|V|jj\rangle_{J_K} \quad (8)$$

When considering gamma-ray emission involving multipolarity L and denoted by the symbol σ, the transition probability λ(σL) is expressed as follows [19]:

$$\lambda(\sigma L,\ J_i \longrightarrow J_f) = \frac{8\pi\,(L+1)}{\hbar L[(\,2L+1)!!]^2}\left(\frac{E_\gamma}{\hbar c}\right)^{2L+1}B(\sigma L,J_i \longrightarrow J_f) \quad (9)$$

where *B(σL)* is the reduced transition probability and Eγ is the γ-ray energy.

The reduced matrix element $\langle\psi\, f\,\|M(\sigma L)\|\psi i\rangle$ can be used to express the reduced transition probability [18]:

$$B(\sigma L, J_i \longrightarrow J_f) = \frac{1}{2J_i+1}\,|\langle\psi\, f\ \|\ M(\sigma L)\ \|\ \psi i\rangle|^2 \quad (10)$$

3. Results and Discussion

The ^{19}O nucleus calculations are executed through the shell model within the NuShellX@MSU code for Windows [7]. This involves employing the sdpn model space coupled with effective interactions, specifically USDEPN and WCPN. Within the sdpn model space, there are three orbitals ($0d_{5/2}$, $1s_{1/2}$, and $0d_{3/2}$) situated above the closed core of ^{16}O, with three neutrons for the given nucleus.

The primary objective of the present study is to carry out computations for energy levels, decrease electromagnetic transition probabilities, and the charge density distribution for the ^{19}O nucleus. These computations are conducted using the harmonic oscillator potential (HO) with parameter b > 0. The corresponding single-particle energies are ($0d_{3/2}$= 1.8896,$1s_{1/2}$ - 3.4150,$0d_{5/2}$ - 4.1692) for the USDEPN interaction, and ($0d_{3/2}$ = 1.64658,$1s_{1/2}$ = -3.16354,$0d_{5/2}$ - 3.9478) for the WCPN interaction.

3.1 Energy Levels

Per the shell model's description, the foundational configuration of the ^{19}O nucleus involves a ^{16}O nucleus in a closed state, encircled by three neutrons positioned outside this closed shell. These neutrons are arranged within the sdpn shell, and their arrangement corresponds to quantum numbers J = 0^+ and T = 1.5. By employing the NuShellX@MSU code within the sdpn shell to implement the interaction USDEPN onto the ^{19}O nucleus, and after comparison with experimental data, we drew the following conclusions:

Upon comparison with the available empirical data, the total angular momentum and parity of the ground state level $5/2\,^+_1$ were found to be in agreement.

A good agreement was obtained for the values of the theoretically calculated MeV energies (0.12,1.602, 2.347, 2.889, 3.209, 6.13) MeV corresponding to the angular momentum ($3/2^+_1$, $1/2^+_1$, $9/2^+_1$, $7/2^+_1$, $5/2^+_2$, $3/2^+_2$), when compared with available experimental data. Additionally, through our calculations, we were able to obtain an agreement that is appropriate for the energy value (3.814, 10.697) MeV calculated theoretically, which corresponds to the angular momentum $3/2^+_2$, $7/2^+_4$ but with a different parity.

The parity of the energy levels at 5.384 and 5.007 MeV, corresponding to the angular momenta $9/2^+_2$ and $5/2^+_3$, was determined to be positive.

Our computations indicate that the total angular momentum and parity corresponding to the experimental energy levels at 7.118, 7.242, 7.508, 8.048, 8.916, 9.430, 9.560, 9.930, 11.250, and 11.580 MeV are projected as $7/2^+_2$, $5/2^+_4$, $1/2^+_2$, $11/2^+_1$, $3/2^+_4$, $7/2^+_3$, $5/2^+_5$, $9/2^+_3$, $1/2^+_3$, and $3/2^+_6$, respectively.

Our calculations revealed 16 levels characterized by specific total angular momentum and parity, yet these levels did not align with any existing empirical data. Additionally, it came to our attention that the theoretically derived maximum energy value stands at 21.805 MeV, while the highest practical energy value observed is 11.580 MeV.

As for our comparison with the theoretical results that we obtained from [9], we observed a good agreement for the ground state angular momentum $5/2^+_1$. Also, the agreement was good for all energy levels.

Figure 1 presents a comparison between the experimental data from Ref. [20] and the theoretical predictions for the ^{19}O nucleus, obtained using the USDEPN interaction, alongside the theoretical results from Ref. [9], which employed the USDBPN interaction.

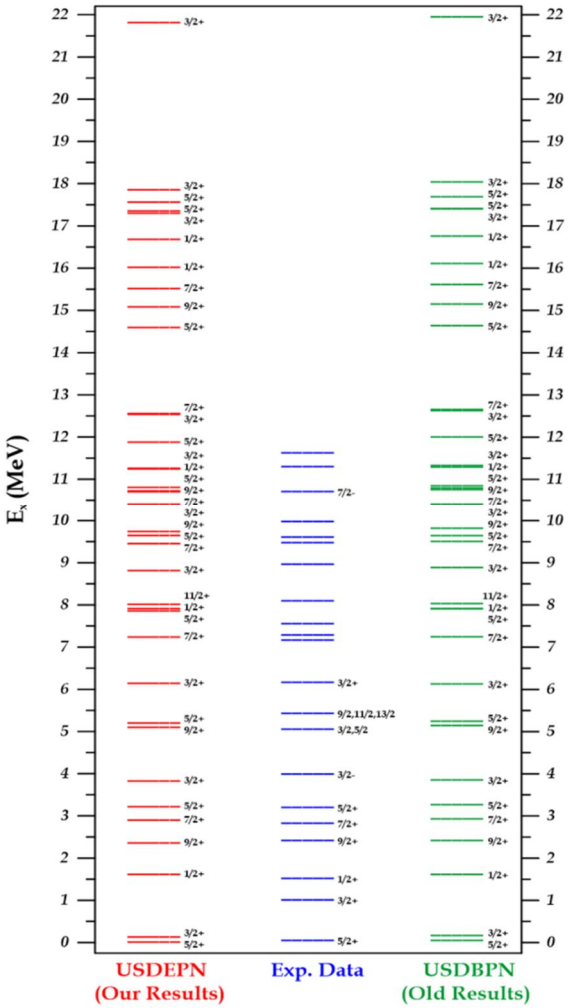

FIG. 1. Comparison of experimental excitation energies from Ref. [20] with our theoretical results using the USDEPN interaction, alongside theoretical results from Ref. [9] employing the USDBPN interaction.

Upon applying the effective interaction WCPN to the ^{19}O nucleus within the sdpn shell, we reached the following conclusions after comparison with experimental data:

Compared with the practical values available, there was a correspondence observed between the total angular momentum and ground state parity of the $5/2^+_1$ level.

Upon comparison with the existing experimental data, a notable concurrence was evident between the theoretically computed energy values (0.294, 1.469, 2.447, 2.96, 3.167, 5.527) MeV and the corresponding angular momenta ($3/2^+_1$, $1/2^+_1$, $9/2^+_1$, $7/2^+_1$, $5/2^+_2$, $3/2^+_3$). Furthermore, our calculations produced acceptable agreement for the energy values 3.747 and 10.253 MeV, corresponding to angular momenta $3/2^+_2$ and $7/2^+_4$, but with a different parity.

The parity for the values of practical energies (5.384, 5.007, 6.466 MeV) corresponding to the angular momenta ($9/2^+_2$, $5/2^+_3$, and $7/2^+_2$) was determined to be positive.

Our computations yielded projections indicating that, owing to the convergence between experimental and theoretical values, the total angular momentum and parity corresponding to the experimental energies 7.118, 7.242, 7.508, 8.247, 8.916, 9.064, 9.324, 9.430, and 11.580 MeV are $1/2^+_2$, $5/2^+_4$, $11/2^+_1$, $3/2^+_4$, $5/2^+_5$, $7/2^+_3$, $9/2^+_3$, $3/2^+_5$, and $5/2^+_7$.

From our calculations, we identified 16 levels characterized by specific total angular momentum and symmetry for which no experimental counterparts can be found. Furthermore, we observed a discrepancy in energy values, with the highest practical energy recorded at 11.580 MeV, whereas the theoretical calculation indicated a peak energy of 20.913 MeV.

Our comparison with theoretical results reported in Ref. [9] shows a match for the ground state value of angular momentum $5/2^+_1$. On the other hand, all other energy levels show good consistency.

As for the highest practical value for our calculations, it was 20.913 MeV. As for the highest practical value for the theoretical calculations that were compared to it, it was 21.902 MeV.

Figure 2 presents a comparison between the experimental findings sourced from Ref. [20] and the theoretical outcomes concerning the ^{19}O nucleus, utilizing the WCPN interaction, along with the theoretical data from Ref. [9] based on the USDBPN interaction.

3.2 Electromagnetic Transition Probabilities

In this study, we undertook the computation of electromagnetic transition probabilities B(E2) and B(M1) using a harmonic oscillator potential (HO, b) with b > 0 for each transition. This was accomplished by applying the USDEPN and WCPN interactions within the sdpn model space for the ^{19}O nucleus. Introducing the primary polarization effect involved the selection of effective charges for protons and neutrons: e_p = 1.410, e_n = 0.410 for the USDEPN interaction, and e_p = 1.400, e_n = 0.400 for the WCPN interaction. Moreover, we adjusted the g factor to achieve conformity with practical values pertaining to the ground state magnetic transitions, to become g_sp = 8.500 and g_s n = 8.500 and g_sp = 9.950 and g_sn = 9.950 for USDEPN and WCPN interactions, respectively.

Regarding the interaction USDEPN, when we compared our results with the experimental results, we observed favorable agreement in electric transitions B(E2) $1/2_1 \rightarrow 5/2_1$, B(E2) $9/2_1 \rightarrow 5/2_1$. Similarly, magnetic transition compatibility was notable for the transitions B(M1) $3/2_1 \rightarrow 5/2_1$, B(M1) $1/2_1 \rightarrow 3/2_1$, aligning well with existing experimental data [20]. Additionally, our calculations unveiled new transitions for which no experimental values have been documented thus far. On the other hand, when we compared our calculations with the theoretical results we obtained from the Ref. [9], we found acceptable agreement for the transitions B(E2) $1/2_1 \rightarrow 5/2_1$, B(E2) $9/2_1 \rightarrow 5/2_1$, B(E2) $7/2_1 \rightarrow 5/2_1$, B(E2) $7/2_1 \rightarrow 9/2_1$, B(E2) $11/2_1 \rightarrow 9/2_1$, B(E2) $11/2_1 \rightarrow 7/2_1$. We also noticed the presence of transfers that were not calculated theoretically. As for magnetic transitions, no comparative theoretical data were available.

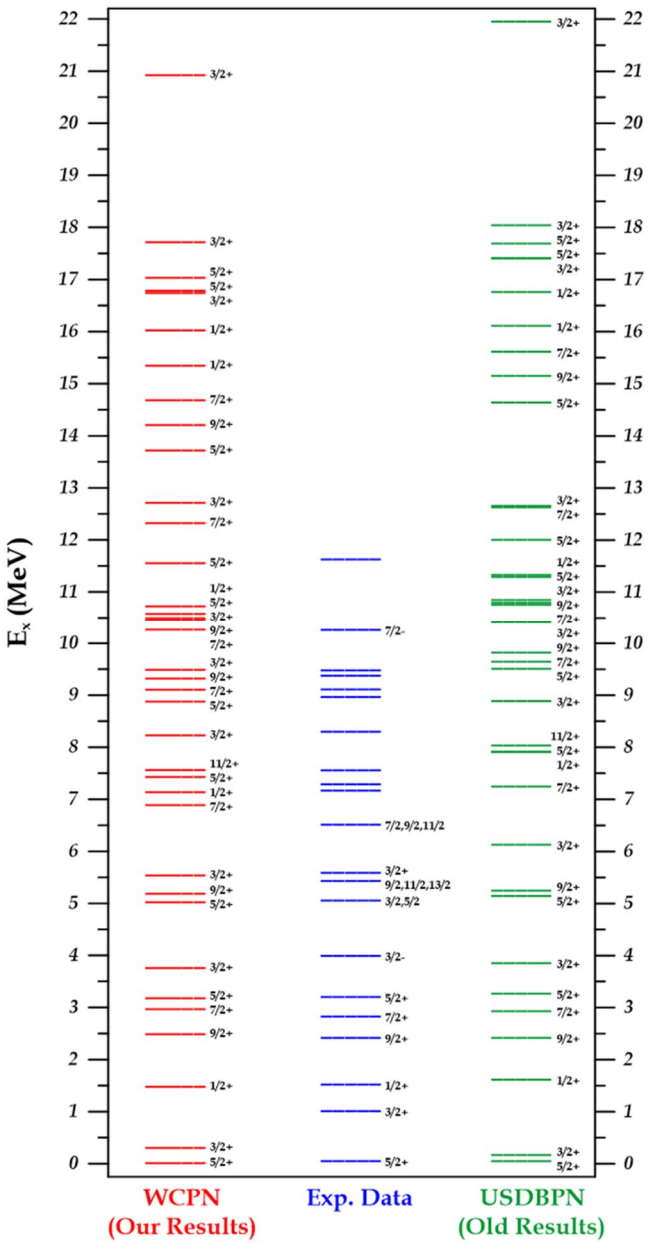

FIG. 2. Comparison of the experimental excitation energies taken from Ref. [20] with our theoretical results using WCPN interaction and theoretical results from Ref. [9] using USDBPN interaction.

Simultaneously, upon applying the WCPN interaction and comparing the results with experimental data, we observed favorable agreement for several transitions, including B(E2) $1/2_1 \rightarrow 5/2_1$, B(E2) $9/2_1 \rightarrow 5/2_1$, B(M1) $3/2_1 \rightarrow 5/2_1$, B(M1) $1/2_1 \rightarrow 3/2_1$ [20]. Additionally, our theoretical calculations predicted new transitions that have not yet been experimentally confirmed. On the other hand, when we compared our calculations with the theoretical results we obtained from the reference [9], we found acceptable agreement for the transitions B(E2) $1/2_1 \rightarrow 5/2_1$, B(E2) $9/2_1 \rightarrow 5/2_1$, B(E2) $7/2_1 \rightarrow 5/2_1$, B(E2) $7/2_1 \rightarrow 9/2_1$, B(E2) $11/2_1 \rightarrow 9/2_1$, B(E2) $11/2_1 \rightarrow 7/2_1$. We also noticed the presence of transfers that were not calculated theoretically. Regarding magnetic transitions, no comparative theoretical data were available in the referenced literature.

Table 1 presents a comparison between some of our theoretical values calculated using effective interaction USDEPN and both the practical values [20] and the theoretical results we obtained from Ref. [9] (using USDBPN interaction) for electric transitions.

Table 2 shows a comparison between some of our theoretical values using effective interaction USDEPN and the practical values [20] for magnetic transitions.

Table 3 compares some of our theoretical values computed using effective interaction WCPN with both the practical values [20] and the theoretical results (USDBPN interaction) we obtained from Ref. [9] for electric transitions. Finally, Table 4 shows a comparison between some of our theoretical values using effective interaction WCPN and the practical values [20] for magnetic transitions.

TABLE 1. Comparison of the B(E2) outcomes (in units of e^2 fm^4) for the ^{19}O isotope, computed using the USDEPN interaction, with the experimental data from Ref. [20] and theoretical results from Ref. [9] based on the USDBPN interaction

Ji→Jf	B(E2), Our results (e^2fm^4) for USDEPN *e_p 1.410= e_n=0.410*	B(E2) Exp. results (e^2fm^4)	B(E2) Theor. results (e^2fm^4) USDBPN
$1/2_1 \rightarrow 5/2_1$	1.748	1.747	10.75
$9/2_1 \rightarrow 5/2_1$	2.022	> 3.012	12.49
$3/2_1 \rightarrow 5/2_1$	7.6150	-----	64.63
$7/2_1 \rightarrow 5/2_1$	2.829	-----	16.579
$7/2_1 \rightarrow 9/2_1$	2.6630	-----	16.23
$5/2_2 \rightarrow 5/2_1$	0.6344	-----	-----
$11/2_1 \rightarrow 9/2_1$	0.8306	-----	5.095
$11/2_1 \rightarrow 7/2_1$	1.2670	-----	7.874
$1/2_1 \rightarrow 3/2_1$	0.4816	-----	-----

TABLE 2. Comparison of the B(M1) outcomes (in units of μ^2) for the ^{19}O nucleus, computed using the USDEPN interaction, with experimental data from Ref. [20].

Ji→Jf	B(M1), Our results USDEPN g_Sp = 8.500, g_Sn = - 8.500	B(M1) Exp. results μ^2
$3/2_1 \rightarrow 5/2_1$	0.1357	0.158
$1/2_1 \rightarrow 3/2_1$	0.1373	0.017
$7/2_1 \rightarrow 5/2_1$	0.1236	-----
$5/2_2 \rightarrow 5/2_1$	0.0099	-----
$5/2_2 \rightarrow 3/2_1$	0.6131	-----
$11/2_1 \rightarrow 9/2_1$	1.1400	-----

TABLE 3. Comparison of the B(E2) outcomes (in units of e^2 fm^4) for the ^{19}O isotope, computed using the WCPN interaction, with the experimental results from Ref. [20] and theoretical results from Ref. [9] using the USDBPN interaction

Ji→Jf	B(E2) Our results(e^2fm^4) for WCPN *e_p 1.400, e_n=0.400*	B(E2) Exp. results (e^2fm^4)	B(E2) Theory. results (e^2fm^4) USDBPN
$1/2_1 \rightarrow 5/2_1$	1.7300	1.747	10.75
$9/2_1 \rightarrow 5/2_1$	1.910	> 3.012	12.49
$3/2_1 \rightarrow 5/2_1$	6.9560	-----	64.63
$7/2_1 \rightarrow 5/2_1$	2.6990	-----	16.579
$7/2_1 \rightarrow 9/2_1$	2.3740	-----	16.23
$5/2_2 \rightarrow 5/2_1$	0.6227	-----	-----
$11/2_1 \rightarrow 9/2_1$	0.7803	-----	5.095
$11/2_1 \rightarrow 7/2_1$	1.5830	-----	7.874
$1/2_1 \rightarrow 3/2_1$	0.4823	-----	-----

TABLE 4. Comparison of the B(M1) outcomes (in units of μ^2) for the ^{19}O nucleus, computed using the WCPN interaction, with experimental data from Ref. [20]

Ji→Jf	B(M1), Ours. results WCPN g_sp=9.950,g_sn=- 9.950	B(M1) Exp. results μ^2
$3/2_1 \rightarrow 5/2_1$	0.1056	0.158
$1/2_1 \rightarrow 3/2_1$	0.3058	0.017
$7/2_1 \rightarrow 5/2_1$	0.2204	
$5/2_2 \rightarrow 5/2_1$	0.0025	
$5/2_2 \rightarrow 3/2_1$	0.8348	
$11/2_1 \rightarrow 9/2_1$	1.4690	

3.3 Charge Density Distribution

Figure 3 illustrates the distribution of charge density within the ^{19}O nucleus. As shown, the value of the charge density at the center of the nucleus is 0.08736 e.fm^{-3}. Then it decreases to r = 4.5 fm, and then its value is fixed at zero.

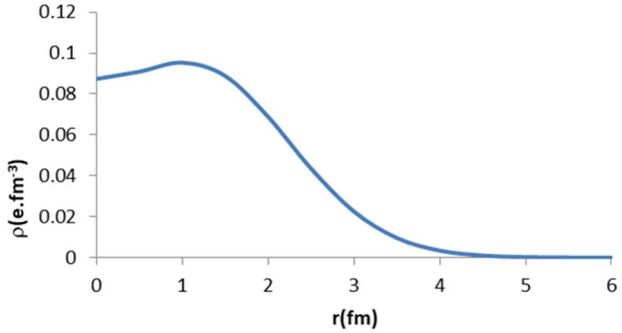

FIG. 3. The charge density distribution of the ^{19}O nucleus.

4. Conclusions:

Utilizing the NuShellX@MSU code within the sdpn shell and employing the effective interactions of USDEPN and WCPN, we conducted calculations concerning energy levels, electromagnetic transition probabilities, and charge density distribution for the ^{19}O nucleus. The present study effectively demonstrates that these interaction files align harmoniously with the available experimental data. Our computations confirmed a multitude of energy levels for both interactions, unveiling novel energy states. The congruence between the B(E2) and B(M1) values and the experimental results was also noteworthy. Furthermore, our calculations led us to conclude that the value of the charge density at the center of the nucleus is 0.08736 e.fm^{-3}, then it gradually diminishes, and eventually stabilizes at zero. Overall, these findings confirm that applying the shell model configuration mixing within the sdpn shell provides reliable and satisfactory results.

References:

[1] Obeed, F.H., Jordan J. Phys., 14 (2021) 25.

[2] Saeed, M., Nemati, G.B., and Shayan, S.N., Nucl. Sci., 2 (2017) 1.

[3] Mohammadi, S. and Kafash, E., Asian J. Eng. Technol. Innov., 2 (2014) 18.

[4] Brown, B.A. et al., MSU-NSCL Rep., 1289 (2004).

[5] Caurier, E. and Nowacki, F., Acta Phys. Pol. B, 30 (1999) 705.

[6] Brown, B. and Rae, W., NuShell@MSU MSU-NSCL Rep., (2007).

[7] Brown, B. and Rae, W., Nucl. Data Sheets, 120 (2014) 115.

[8] Hasan, A. and Abed, H., Nucl. Phys. At. Energy, 24 (2023) 219.

[9] Hasan, A., Ukr. J. Phys., 63 (2018) 189.

[10] Itaco, N., Coraggio, L., Covello, A., and Gargano, A., J. Phys.: Conf. Ser., 336 (2011) 012008.

[11] Coraggio, L. and Itaco, N., Front. Phys., 8 (2020) 345.

[12] Hasan, A.K. and Abed, H.H., AIP Conf. Proc., 2977 (2023) 030017.

[13] Condon, E.U. and Odabasi, H., Atomic Structure: CUP Archive, (1980).

[14] De-Shalit, A. and Talmi, I., "Nuclear Shell Theory", Vol. 14, (Academic Press, 2013).

[15] Elliott, J.P. Proc. R. Soc. Lond. A Math. Phys. Sci., 245 (1958) 128.

[16] Bayman, B.F. and Lande, A., Nucl. Phys., 77 (1966) 1.

[17] Lawson, R., "Theory of the Nuclear Shell Model", (1980).

[18] Brussaard, P.J. and Glaudemans, P.W.M., "Shell-Model Applications in Nuclear Spectroscopy", (North-Holland publishing company, 1977).

[19] Preston, M.A., "Structure of the Nucleus", (CRC Press, 2018).

[20] Tilley, D., Weller, H., Cheves, C., and Chasteler, R., Nucl. Phys. A, 595 (1995) 1.